Stability of a Non-Cohesive Soil Under Elliptic Upward Seepage

Stabilité d'un sol pulvérulent dans le cas d'infiltration elliptique ascendante

by Z. BAŽANT, Jr., Professor of Foundation Engineering, Technical University, Karloro nám. 17, Prague, Czechoslovakia

Summary

The authors study the stability of non-cohesive soils under weirs and cofferdams subject to seepage. The object of the investigation was to find methods of preventing piping. A mathematical solution is given for the case where stability is governed by shear and when the flow lines are homofocal ellipses with the toe of the structure as their focus.

The required depth of foundation is given by equations (19) to (22). Table 2 and the graphs in Figs. 5–6 obviate the need for calculation. We are able to neglect the angle of internal friction in equilibrium studies of structures not subject to vibration but this angle has a marked effect on weirs which are subject to vibration.

The stability of structures with shallow foundations depends also on the contact pressure. The results obtained theoretically were checked by tests.

Sommaire

Nous considérons l'équilibre limite des sols pulvérulents sous les barrages et batardeaux dans les cas d'infiltration d'eau. Le but de notre étude est la recherche de mesures propres à empêcher la formation du renard. Une solution mathématique est proposée pour le cas où l'équilibre limite peut se développer par cisaillement et lorsque les lignes de courant sont des ellipses homofocales dont le pied aval de l'ouvrage est le foyer. L'estimation de la fiche, soit la profondeur de la fondation se fait au moyen des équations (19) à (22), du Tableau 2 et des graphiques des Fig. 5–6, qui remplacent complètement le calcul. Nous pouvons négliger l'angle de frottement interne dans l'étude de l'équilibre des ouvrages non vibrants, par contre les barrages vibrants sont affectés d'une manière sensible par cet angle. L'équilibre des ouvrages de faible profondeur dépend en outre de la pression à la surface de contact. Les résultats obtenus théoriquement furent contrôlés par les essais.

We shall consider the stability of a weir or sheet pile wall founded on a non-cohesive subsoil. The failure studied here is known as piping. In order to avoid piping, the foundations of the structure on the downstream side must reach the proper depth. The design of this depth is the purpose of the following article.

History

The first solution of stability was worked out in India in 1902. This is the well-known *Bligh* creep-head theory which was improved by *E. W. Lane* (1934). The second solution, the liquefaction method, was developed by *K. Terzaghi* (1922). He assumed the liquefaction due to the seepage pressure to be the cause of failure. *L. F. Harza* (1934) derived from this solution the method of critical gradient now in general use.

The author studied the case of an elliptic seepage under a sheet pile wall, where the exit gradient is not the maximum gradient (*Bažant*, 1940). He came to a result similar to that of *K. Terzaghi* (1943) in his new solution.

Failure by Shear

The solution studied in this article is known as the shear method, and assumes that the failure is due to shear. Let us consider a weir or cofferdam founded on a stratum of non-cohesive soil (Fig. 1). The seepage follows the course of flow lines and causes the seepage pressure. The seepage pressure is dangerous only on the downstream side, where it shows an upward direction, and therefore lifts the soil grains. We assume that the failure by shear occurs along the circular cylindrical surface at the right of the hatched segment-shaped area in Fig. 1.

The forces acting on the segment are the total weight of soil and water, the neutral forces on the perimeter and the weight of the riprap filter on the surface of the segment. These forces are in equilibrium with the effective forces along the wall on

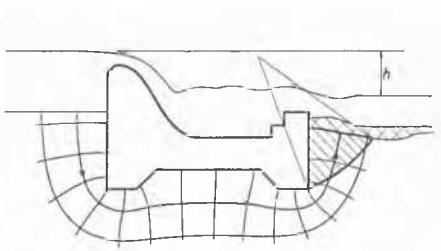

Fig. 1 Failure at the Toe of Weir
Rupture d'équilibre dans la région avoisinant la base aval du déversoir

the left and along the failure surface on the right. The concept of forces using the total weight and boundary neutral forces supersedes the original concept of submerged weight and seepage pressure, and simplifies the solution (*Taylor*, 1948).

The stability condition of the segment requires that the shear strength along every possible failure surface should be greater than the shear stress. The shape of the failure surface was assumed to be cylindrical. This shape of the failure surface is commonly used in the analysis of the stability of slopes and

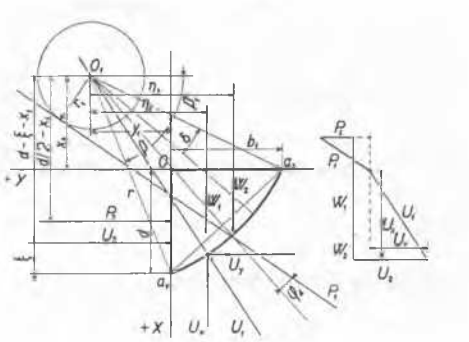

Fig. 2 Elements of the Stability Analysis
Eléments de calcul de la stabilité à l'équilibre limite

was also suggested by *Grishin* (1938) for our case. *Grishin* assumed that the structure on the surface of the soil and the arc of failure passed through the heel. The tests showed that this was not correct. The author suggests a structure founded below the surface and the arc passing through the toe of this structure. This concept was found to agree with the tests and also was easy to solve by charts.

To render our solution applicable it was necessary to make the following assumptions:

(1) The structure of soil is stable with proper filter characteristics.
(2) The soil is homogeneous and the cavities under the base are refilled or the erosion stopped.
(3) The horizontal thrust of water is not taken into account and is transmitted to the subsoil along the base of the weir, or in the case of a sheet pile wall it is counterbalanced by bracing.
(4) The failure is caused by shear.
(5) The flow is two-dimensional.
(6) The failure surface is cylindrical.
(7) The stability of downstream side is the governing factor.
(8) The cylindrical surface passes through the toe.
(9) The surface of the downstream side is horizontal.

The validity of these assumptions was proved by tests and by application of the theory in practice.

Mathematical Analysis of Equilibrium (*Bažant*, 1953)

The author has worked out a graphical method for the general case of seepage using the friction-circle method. The procedure is rather cumbersome and the results are not accurate enough. To avoid this difficulty he analysed the case mathematically. The mathematical analysis is based on flow lines on the downstream side which are assumed to be ellipses with a common focus at the toe.

The forces and distances considered in the analysis of equilibrium are shown in Fig. 2. The fundamental case does not take into account the riprap filter. Thus the forces are: the total weights W_1, W_2, the neutral forces U_1, U_2 and effective forces P_1, P_2. Total weights and neutral forces are in equilibrium with the effective forces P_1, P_2 (Fig. 2).

Each effective force has three unknowns: amount, direction and point of application. There are altogether six unknowns for which we have only three fundamental equations of equilibrium. The case is therefore three times statically indeterminate. We chose as the static indeterminates the amount, the direction and the point of application of the force P_2. We resolve them from the deformation conditions independently from P_1. Considering P_2 as known we determine P_1 by three fundamental equations of equilibrium.

The equilibrium moment about the axis 0_1 of the circular failure surface is given by:

$$P_1 r_1 = P_2\left(\frac{d}{2} - x_1\right) + U_2(d - \xi - x_1) - W_1\eta_1 - W_2\eta_2 \quad (1)$$

From the equilibrium of horizontal and vertical components follows the resultant:

$$P_1^2 = (P_2 + U_2 - U_y)^2 + (W_1 + W_2 - U_x)^2 \quad (2)$$

Inserting P_1 into (1) we obtain the radius of the friction circle

$$r_1 = \frac{P_2(d/2 - x_1) + U_2(d - \xi - x_1) - W_1\eta_1 - W_2\eta_2}{\sqrt{(P_2 + U_2 - U_y)^2 + (W_1 + W_2 - U_x)^2}} \quad (3)$$

The central angle of the segment being small we assume P_1 tangential to the friction circle. Thence we obtain for the given radius r of the circular arc the angle φ_d of obliquity of force P_1

$$\sin\ \varphi_d = \frac{r_1}{r} \quad (4)$$

The angle φ_d is the developed shear characteristics. We investigate several trial circles with centres in the upper left quadrant. Then by a special method we find the trace of the superficies whose heights are φ_d assigned to the respective centres of circles. This enables us to determine the angle max φ_d, expressing the greatest stress which the soil may withstand for the given structure.

Analytical Determination of Forces.

The forces and distances entering into the analysis are shown in Fig. 2. Axis $+X$ is going downward, and $+Y$ leftward.

The total weights are:

$$W_1 = \frac{1}{2}\gamma_t b_1 d \quad (5)$$

$$W_2 = \frac{1}{2}\gamma_t r^2(\beta - \sin\beta) \quad (6)$$

The arms are:

$$\eta_1 = \frac{b_1}{3} + y_1,$$

$$\eta_2 = \frac{b_1}{2} + y_1 + r\left[\frac{4}{3}\frac{\sin^2\beta/2}{\beta - \sin\beta} - \cos\beta/2\right]\cos\left(\frac{\beta}{2} + \beta\right)$$

The sum $W_1\eta_1 + W_2\eta_2$ is simply given by the equation:

$$W_1\eta_1 + W_2\eta_2 = -\frac{1}{2}\gamma_t\left(\frac{x_1}{d} - \frac{2}{3}\right)d^3 \quad (7)$$

γ_t expresses the unit weight of combined soil and water.

The neutral stress is found by the theory of seepage as follows:

$$u_w = \gamma_w\left(\frac{2h_r}{\pi}\Phi + h_r + x\right) \quad (8)$$

The neutral force along the wall which is the resultant of neutral stresses, is given by:

$$U_2 = \gamma_w \int_0^d \left(\frac{2h_r}{\pi} \Phi + h_r + x \right) dx \quad . . \tag{8a}$$

γ_w is the unit weight of water and h_r the pressure head at the toe. h_r is represented by the distance between the segment surface and the water surface in the imaginary standpipe, h_r being the resting fraction of h. Φ is the potential. For elliptic flow lines with a common focus at the toe the potential Φ is the parameter of the hyperbolic equipotential lines whose equation is:

$$\frac{x^2}{d^2 \cos^2 \Phi} - \frac{y^2}{d^2 \sin^2 \Phi} = 1 \tag{8b}$$

Along the wall $y = 0$ and the potential

$$\Phi = -\arccos \frac{x}{d} \tag{9}$$

The integration of equation (8) follows:

$$U_2 = -\gamma \frac{2h_r}{w\,\pi} \int_0^d \arccos \frac{x}{d}\, dx + \gamma_w \int_0^d (h_r + x) dx \tag{10}$$

The first integral is:

$$\int_0^d \arccos \frac{x}{d}\, dx = \left[x \arccos \frac{x}{d} - \sqrt{d^2 - x^2} \right]_0^d$$

and then the neutral force along the wall

$$U_2 = \left(1 - \frac{2}{\pi}\right) \gamma_w h_r d + \frac{1}{2} \gamma_w d^2 \quad . . \tag{11}$$

The moment arm of U_2 is given by $d - \xi - x_1$ in which the term ξ can be derived from the equilibrium of static moments about a_1:

$$\xi \left(1 - \frac{2}{\pi}\right) \gamma_w h_r d + \xi \frac{1}{2} \gamma_w d^2 =$$

$$= -\gamma_w \frac{2h_r}{\pi} \int_0^d (d - x) \arccos \frac{x}{d}\, dx + \gamma_w \int_0^d (d - x)(h_r + x) dx$$

Because

$$\int_0^d x \arccos \frac{x}{d}\, dx = \left[\frac{2x^2 - d^2}{4} \arccos \frac{x}{d} - \frac{x}{4} \sqrt{d^2 - x^2} \right]_0^d$$

it follows that

$$\xi = \frac{3h_r (3\pi - 8) + 2\pi d}{12h_r (\pi - 2) + 6\pi d} \tag{12}$$

Approximative Determination of U_x, U_y

It is not possible to solve exactly the components U_x, U_y of the neutral force U_1 along the circular surface, the potential Φ being intricate. We obtain Φ from (8b). Multiplying it by $\sin^2 \Phi$ and replacing the goniometric functions by $\operatorname{tg} \Phi$ we obtain:

$$\frac{x^2}{d^2} \operatorname{tg}^2 \Phi - \frac{y^2}{d^2} = \frac{\operatorname{tg}^2 \Phi}{1 + \operatorname{tg}^2 \Phi}$$

This gives the equation:

$$x^2 \operatorname{tg}^4 \Phi + (x^2 - y^2 - d^2) \operatorname{tg}^2 \Phi - y^2 = 0$$

from which follows in our quadrant the potential given by the equation:

$$\Phi = -\operatorname{arctg} \sqrt{\frac{1}{2x^2} \left[-(x^2 - y^2 - d^2) + \sqrt{(x^2 - y^2 - d^2) + 4x^2 y^2} \right]} \tag{13}$$

This equation gives for $+X$ and $x > d$ the potential $\Phi = 0$ and for $-Y$ the potential $\Phi = -\pi/2$ which both are the known results.

According to (8) the component of the neutral force U_1 in the X direction is:

$$U_x = \gamma_w \int_{\beta_1}^{\beta+\beta_1} \left(\frac{2h_r}{\pi} \Phi + h_r + x \right) \sin (\beta_1 + \delta) r\, d\delta \tag{14}$$

where the coordinates of points along the circular surface

$$x = r \sin (\beta_1 + \delta) + x_1$$

$$y = -r \cos (\beta_1 + \delta / + y_1$$

The integration of (14) gives for the first term:

$$\int_{\beta_1}^{\beta+\beta_1} \frac{2h_r}{\pi} \Phi \sin (\beta_1 + \delta)\, r\, d\delta = -\frac{2h_r}{\pi} I_1 d$$

I_1 being the sign for integral which it is not possible to express simply with elementar functions. The second term

$$\int_{\beta_1}^{\beta+\beta_1} h_r \sin (\beta_1 + \delta)\, r\, d\delta = -h_r r \left[\cos (\beta_1 + \delta) \right]_{\beta_1}^{\beta+\beta_1} = h_r b_1$$

The third term

$$\int_{\beta_1}^{\beta+\beta_1} x \sin (\beta_1 + \delta)\, r\, d\delta = \int_{\beta_1}^{\beta+\beta_1} r^2 \sin^2 (\beta_1 + \delta) d\delta + \int_{\beta_1}^{\beta+\beta_1} x_1 r \sin (\beta_1 + \delta) d\delta$$

$$= \frac{r^2}{2} \left[(\beta_1 + \delta) - \frac{1}{2} \sin 2 (\beta_1 + \delta) \right]_{\beta_1}^{\beta+\beta_1} - x_1 r \left[\cos (\beta_1 + \delta) \right]_{\beta_1}^{\beta+\beta_1}$$

$$= \frac{1}{2} r^2 \beta - \frac{1}{2} r^2 \cos (2\beta_1 + \beta) \sin \beta + 2x_1 r \sin \left(\beta_1 + \frac{\beta}{2} \right) \sin \frac{\beta}{2}$$

On inserting $2x_1 r = -2r^2 \sin \beta_1$ developing the goniometric functions and adding $-\frac{1}{2} r^2 \sin \beta + \frac{1}{2} r^2 \sin \beta$, we obtain after some transformations:

$$= \frac{1}{2} r^2 (\beta - \sin \beta) + \frac{1}{2} r^2 \left[\cos \beta_1 - \cos (\beta + \beta_1) \right]$$

$$\left[\sin (\beta + \beta_1) - \sin \beta_1 \right]$$

Using the geometric relations (Fig. 2) we obtain simply

$$= \frac{1}{2} r^2 (\beta - \sin \beta) + \frac{1}{2} b_1 d$$

These three terms together multiplied by γ_w finally give:

$$U_x = -\gamma_w \frac{2h_r}{\pi} I_1 d + \gamma_w b_1 \left(h_r + \frac{d}{2} \right) + \gamma_w \frac{r^2}{2} (\beta - \sin \beta) \tag{15}$$

The component of the neutral force U_1 in the Y direction

$$U_y = \gamma_w \int_{\beta_1}^{\beta+\beta_1} \left(\frac{2h_r}{\pi} \Phi + h_r + x \right) \cos (\beta_1 + \delta) r\, d\delta$$

The integration gives for the first term

$$\int_{\beta_1}^{\beta+\beta_1} \frac{2h_r}{\pi} \Phi \cos (\beta_1 + \delta)\, r\, d\delta = -\frac{2h_r}{\pi} I_2 d$$

where I_2 is again the sign for unsolved integral. The second term is given by:

$$\int_{\beta_1}^{\beta+\beta_1} h_r \cos(\beta_1+\delta)\, r\,d\delta = h_r r\,[\sin(\beta_1+\delta)]_{\beta_1}^{\beta+\beta_1} = h_r d$$

The third term:

$$\int_{\beta_1}^{\beta+\beta_1} x\cos(\beta_1+\delta)\, r\,d\delta = \int_{\beta_1}^{\beta+\beta_1} r^2 \sin(\beta_1+\delta)\cos(\beta_1+\delta)\,d\delta +$$

$$+ \int_{\beta_1}^{\beta+\beta_1} x_1 r \cos(\beta_1+\delta)\,d\delta$$

$$\int = \frac{r^2}{2}\,[\sin^2(\beta_1+\delta)]_{\beta_1}^{\beta+\beta_1} + x_1 r\,[\sin(\beta_1+\delta)]_{\beta_1}^{\beta+\beta_1}$$

$$\int = \frac{1}{2} r^2 \sin(2\beta_1+\beta)\sin\beta + 2x_1 r \cos\left(\beta_1+\frac{\beta}{2}\right)\sin\frac{\beta}{2}$$

On inserting $2x_1 r = -2r^2 \sin\beta_1$, and developing the goniometric functions we obtain:

$$\int = \frac{1}{2} r^2 \left[2\sin^2\beta_1 (1-\cos\beta-\frac{1}{2}\sin^2\beta) + \right.$$

$$\left. + 2\sin\beta_1\cos\beta_1\sin\beta(\cos\beta-2) + \cos^2\beta_1\sin^2\beta\right] = \frac{1}{2} d^2.$$

These three terms together multiplied by γ_w give:

$$U_y = -\gamma_w \frac{2h_r}{\pi} I_2 d + \gamma_w h_r d + \frac{1}{2}\gamma_w d^2 \qquad (16)$$

In equations (15) and (16) the terms are

$$I_1 = \int_{\beta_1}^{\beta+\beta_1} \Phi \sin(\beta_1+\delta)\, r\,d\delta$$

$$I_2 = \int_{\beta_1}^{\beta+\beta_1} \Phi \cos(\beta_1+\delta)\, r\,d\delta$$

which we were not able to integrate analytically and therefore computed them approximately. Table 1 shows the extract of the detailed tables for I_1 and I_2.

Table 1

x_1/d	*Function* I_1				*Function* I_2			
	y_1/d				y_1/d			
	30	*20*	*10*	*0*	*30*	*20*	*10*	*0*
— 55	1,99	3,01			1,112	1,165		
— 45	1,607	2,44	4,61		1,088	1,139	1,235	
— 30		1,592	3,10			1,089	1,177	
— 20			2,07	7,93			1,123	1,413
— 10			1,037	5,39			1,054	1,367
0			0,039	0,785			1,001	1,183

Determination of P_2

The statically indeterminate effective force P_2 along the wall requires special investigation. From the deformation conditions of the segment which are comparable to the deformation of the soil behind the sheeting of the trenches (*Ohde*, 1938) we conclude that the amount of P_2 equals the active earth pressure

$$P_2 = \frac{1}{2}\gamma_b'' d^2 \operatorname{tg}^2\left(45° - \frac{\varphi_d}{2}\right) \qquad (16)$$

where the unit weight reduced by seepage pressure is:

$$\gamma_b'' = \gamma_t - \frac{U_r}{\frac{1}{2} b_1 d + \frac{1}{2} r^2 (\beta - \sin\beta)} \qquad (17)$$

The angle φ_d is the angle we sought. We attribute to it an arbitrary value and correct it by trial until the assumed φ_d equalled the computed one. The direction of P_2 is assumed to be horizontal which neglects the friction along the wall. The point of application of P_2 was chosen in the centre of the wall.

Result of the Mathematical Analysis

The analysis of max φ_d was made for the chosen specific gravities $G_t = \gamma_t/\gamma_w$ and the chosen relative pressure heads h_r/d. The result is advantageous by plotted in the form:

$$\frac{h_r}{d} = f(\varphi, G_t) \qquad (18)$$

This function is shown in Fig. 3. On the limit of equilibrium the developed maximal angle max φ_d may equal the angle of

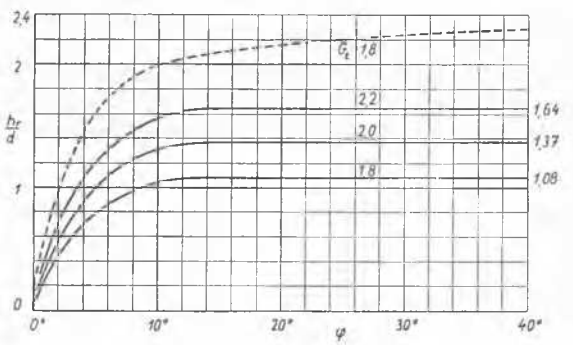

Fig. 3 Chart of Relative Pressure Heads h_r/d
Diagramme de charge relative au pied h_r/d

internal friction φ which is therefore inserted into (18). Fig. 3 shows the maximal relative pressure head h_r/d for a soil with given φ and G_t. The broken line represents the case of a soil on whose surface a surcharge (riprap filter) of the magnitude of $\gamma_w d/2$ is applied.

Design of the Depth of Foundation

The method of limit design is advocated because it combines the greatest load and the smallest strength. The coexistence is considered admissible offering only very slight probability. The load is represented by the pressure head h_r at the toe. We assume that the limit load is the load at the beginning of greater displacements of soil grains. We conclude from the result of stereophotographic measurements (*Bažant*, 1949) that the coefficient of loading, the ratio K_1 of the head h_r on the limit of stability to the head h_e at the beginning of grater displacements is 1.4 for temporary structures and 1.7 for permanent ones. For a sheet pile wall we choose $K_1 = 2$, which takes their flexibility and permeability into account. We take approximately $K_1 = 1$ for cohesive soils. As h is the real head, we insert $K_1 h$ the head at the beginning of greater displacements into the design.

The strength is characterised by G_t and φ. We suppose 1.8 to be the smallest G_t. The smallest angle of internal friction φ for wet soils can be taken to be 38° for well graded sandy gravel, 33° for well graded angular sand, 27° for uniform round sand, and $\varphi < 20°$ for consolidated-quick shear of silt.

The head h_r which it is necessary to know for designing the depth d of *sheet pile walls* can be obtained from the *Mandel* charts (1951), taking into account the different soil levels upstream and downstream and the variable depth of the permeable stratum. If we read $h_r/h = K_3$ in *Mandel*'s charts and the value $h_r/d = K_2$ in Fig. 3, we obtain the permissible re-

lative head

$$K_1 \frac{h}{d} = f(\varphi, G_t, h/d_s) = \frac{K_2}{K_3} \quad . . \qquad (19)$$

Equation (19) holds for a sheet pile wall the horizontal thrust of which is counterbalanced by bracing. For $\varphi > 12°$ we can

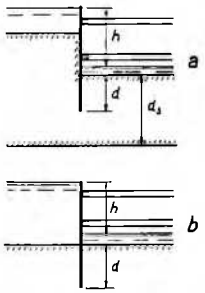

Fig. 4 Braced Sheet Pile Walls
Ecrans étançonnés de palplanches

neglect the influence of φ. Equation (19) holds for each K_1 for certain h/d only. These relative heads h/d are given for $G_t = 1.8$ in Table 2. In this table h = the design head, d =

Table 2

h/d_s		0	0,5	1	1,5	2
h/d	$K_1 = 1{,}4$	1,96	1,92	1,85	1,67	2
	$K_1 = 1{,}7$	1,57	1,52	1,45	1,5	2
	$K_1 = 2$	1,28	1,25	1,18	1,5	2

depth of sheet pile wall, d_s = depth of permeable stratum. The sheet pile wall is illustrated in Fig. 4a. For the sheet pile wall driven in a permeable half-plane in Fig. 4b we have simply

$$K_1 \frac{h}{d} = 2.2 \qquad (20)$$

and for the same case with surcharge $\gamma_w d/2$ on the downstream side we have:

$$K_1 \frac{h}{d} = 4.3 \qquad (21)$$

The design of the downstream depth d of *double wall cofferdams and nonoverflow sections of weirs* uses the charts in Fig. 5, 5a and 5b, which b represents the function

$$K_1 \frac{h}{d} = f(d/2b, \varphi, G_t = 1.8) = \frac{K_2}{K_6} \qquad (22)$$

The charts were derived from Fig. 3 where $h_r/d = K_2$ and from $h_r/h = K_6$ computed by *Khosla, Bose* and *Malhotra* (1936). In these charts besides the known notation 2b denotes the width of the weir or of the cofferdam base. Similar charts can be computed for every possible soil and type of weir foundation. As can be seen from Fig. 3 the maximum value is obtained for $\varphi \geqq 12°$. In order to improve the stability we can take any measure which reduces h_r, such as horizontal drainage, sheet pile wall, filter layer or drainage wells.

The charts in Figs. 6a, b are used for the design of structure on soil whose $G_t = 1.8$ and with a riprap filter which is equal to the overload $\gamma_w d/2$ on the surface of the soil.

The design of the downstream depth d of the *spillway section of weirs* differs with the angle φ_v of internal friction and the depth used. The angle φ_v is the angle at vibration. The vibration is caused by the overflow which vibrates the apron and the downstream soil. The angle φ_v *diminishes* almost to zero

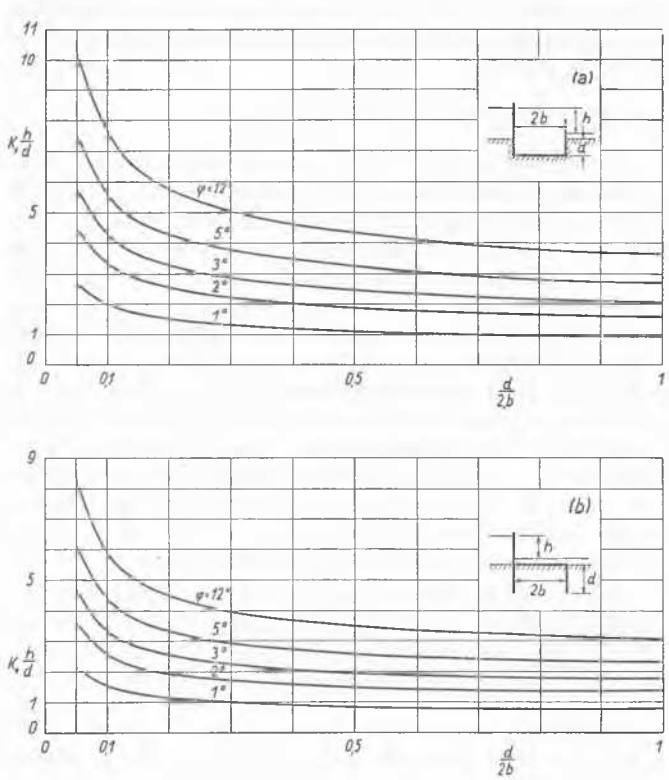

Fig. 5 Charts of Permissible Relative Heads $K_1 h/d$
Diagrammes des différences relatives de niveau admissibles $K_1 h/d$

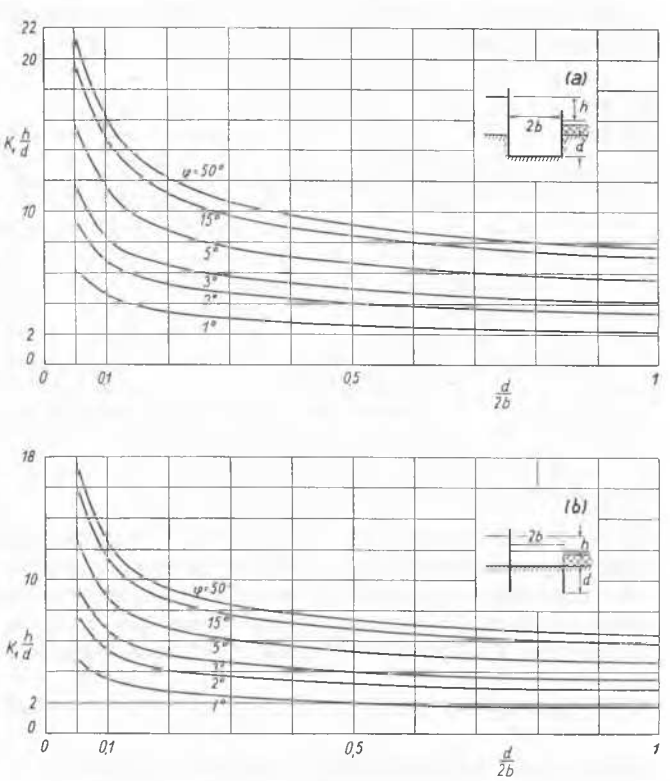

Fig. 6 Charts of Permissible Relative Heads $K_1 h/d$ for Soil Loaded with Riprap Filter
Diagrammes des différences relatives de niveau admissibles $K_1 h/d$ pour un sol avec enrochement à la surface aval

for a small effective pressure and a great vibration. This is the result of tests made by *Tournon* (1948), which are represented in Fig. 7. We suggest provisionally the following values of φ_v:

(1) gravels $\varphi_v = \varphi$,
(2) coarse sands ($d > 0.5$ mm) $\varphi_v = 5°$,
(3) fine sands, such as in the river Indus ($d_{50} = 0.3$ mm) $\varphi_v = 3°$,
(4) sands as are found in the river Volga ($d_{50} = 0.15$ mm) $\varphi_v = 2°$,
(5) fine sands and silts such as in the Nile delta $\varphi_v = 1°$.

It is of course necessary to carry out further tests on φ_v.

The foundation depth d of an overflow section of weir is diminished by scour which can only be predicted by tests. The author believes, however, that the tests carried out with overflow but without seepage do not furnish a reliable depth of scour.

Verification of Theory (*Bažant*, 1953)

The stability of a cohesionless soil in seepage pressure was tested by the author in a flume 30 cm in width, 103 cm in length and 65 cm in height which could be heightened by 100 cm by a special extension element. The flume allowed a head of 80 cm and a weir width of 30 cm. 752 model tests were carried out from 1948 to 1951, firstly to find out the suitable technique of preparing an homogeneous sand with the requested angle of internal friction and then in order to verify the theory. The model tests furnished relative pressure heads h_r/d as shown in Fig. 8. For comparison the theoretical curve is drawn as a broken line.

The result of model tests are satisfactory for $d/2b > 0.1$. Some disagreement occurs for $d/2b < 0.1$. It was found necessary to take into consideration the contact pressure p on the downstream side of the base for these shallow foundations. This is shown in Fig. 9 which presents the result of model tests for the limiting case $d = 0$, h_p denoting head at piping. The variables used in Fig. 9 were determined by dimensionless analysis.

Nevertheless, the computation of stability in seepage of existing structures (Indus, Nile, Volga) disclosed that the theory holds for all practical values of $d/2b$, beginning from $d/2b \geqq 0.05$.

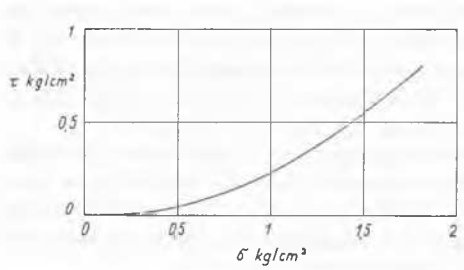

Fig. 7 *Mohr* Diagram for Vibration of Sand (after *Tournon*)
Courbes intrinsèques pour sable vibré (d'après *Tournon*)

The tests disclosed also the mechanics of piping. The stereophotographic measurements (*Bažant*, 1949) of the grains displacement showed that the paths of grains on the downstream side take the direction of the assumed shear lines. This holds until piping takes place. The tests with models founded on surface with model width 300 mm and over distinctly showed the shear of the strip of soil underlying the structure. The shear lasted from 3 to 5 seconds and was sometimes divided into two motions, the initial under the downstream third, and the following under the whole base.

The tests and the successful application of the theory justify the conclusion that the shear method is the useful way of designing the downstream depth of foundation in seepage. The advantage of the shear method is that it furnishes the solution for dynamic cases, with vibration, and so explains

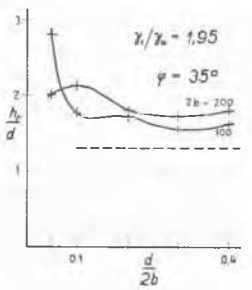

Fig. 8 Results of Piping Model Tests for Deep Foundations
Résultat d'essais sur la formation de renard dans le cas de fondations profondes

satisfactorily the influence of grain sizes on piping which has not bean solved so far. However, for static vibrationless cases the results of analysis using the shear method shown in Fig. 3 are in agreement with the assumption of the liquefaction me-

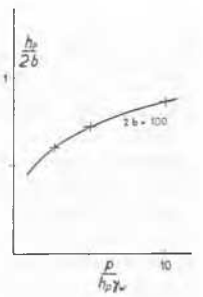

Fig. 9 Results of Piping Model Tests for Shallow Foundations
Résultats d'essais sur la formation de renard dans le cas de fondations de faible profondeur

thod, that is that the angle of internal friction, which is greater than 12°, does not exercise any influence on stability. Here liquefaction method appears as a special case of the shear method.

References

Bažant, Z., Jr. (1940): Grundbruch unter der Spundwand. Die Bautechnik, vol. 18, p. 595.

Bažant, Z., Jr. (1949): Measuring Soil Deformation Caused by the Pressure of the Seepage. XVIIth Int. Navigation Congr., Lisbon. Sect. I, 1st Communication, p. 195.

Bažant, Z., Jr. (1953): Stability of Cohesionless Soil in Curvilinear Upward Seepage (in Czech, with Summaries in Russian, French and English), Prague, Czechoslovak Academy of Sciences, 140 p., 38 figs. In Press, ready in August.

Bliznyak, E. V., Grishin, M. M. et Co. (1938): Hydraulic Structures (in Russian), Moscow, vol. I, p. 272.

Harza, L. F. (1934): Uplift and Seepage under Dams on Sand. Proc. A.S.C.E., vol. 60, p. 990.

L'Hermite, M. R., Tournon, M. G. (1948): La vibration du béton frais. Annales Inst. Tech. Bâtiment et Trav. Publics, février. Nouvelle série, N° 11, p. 45, Fig. 32; p. 46, Fig. 36.

Khosla, R. B. A. N., Bose, N. K., McKenzie Taylor, E. (1936): Design of Weirs on Permeable Foundations, Simla (India), pp. 55, 85.

Lane, E. W. (1934): Security from Under-Seepage: Masonry Dams on Earth Foundations. Proc.A.S.C.E., vol. 60, p. 929.

Mandel, J. (1951): Ecoulement de l'eau sous une ligne de palplanches. Abaques pour la condition de renard. Travaux, Paris, p. 273.

Ohde, J. (1938): Zur Theorie des Erddruckes unter besonderer Berücksichtigung der Erddruckverteilung. Die Bautechnik, Vol. 16, p. 754, Fig. 77.

Taylor, D. W. (1948): Fundamentals of Soil Mechanics, New York, Wiley, p. 200.

Terzaghi, K. (1922): Der Grundbruch an Stauwerken und seine Verhütung. Die Wasserkraft, München, p. 445.

Terzaghi, K. (1943): Theoretical Soil Mechanics. New York, Wiley.